Four-electrode impedance spectrometer for investigation of solid ion conductors

A. Kežionis, P. Butvilas, T. Šalkus, S. Kazlauskas, D. Petrulionis, T. Žukauskas, E. Kazakeviius, and A. F. Orliukas

CrossMark
click for updates

Four-electrode impedance spectrometer for investigation of solid ion conductors

A. Kežionis, P. Butvilas, T. Šalkus,[a)] S. Kazlauskas, D. Petrulionis, T. Žukauskas, E. Kazakevičius, and A. F. Orliukas
Faculty of Physics, Vilnius University, Saulėtekio alėja 9/3, LT-10222 Vilnius, Lithuania

An impedance spectrometer capable of accurately measuring solid ion conducting sample impedance spectra by two- or four-electrode methods in either time or frequency domain has been built. The four-electrode measurement mode is implemented by constructing a differential amplifier with a very high input impedance and common mode rejection ratio over a wide frequency range. All of the measurements can be performed in frequencies ranging from 10 Hz to 2 MHz and sample temperatures up to 800 K. The working principle of the spectrometer as well as its technical parameters and accuracy estimation are presented in this paper. The advantage of four-electrode over two-electrode measurement mode is shown by an example of $Ce_{0.9}Gd_{0.1}O_{1.95}$ solid electrolyte ceramic impedance measurements. © *2013 American Institute of Physics*. [http://dx.doi.org/10.1063/1.4774391]

I. INTRODUCTION

Impedance spectroscopy is a powerful tool used to characterize ionic and mixed electronic-ionic conductors, along with semiconducting and dielectric compounds.[1] It can be utilized in studies of single crystals, ceramics, and glasses, as well as interfaces between different materials.

Usually, in order to obtain the impedance spectra of a material, the current through a sample and the resulting voltage drop are measured by using the same two electrodes for the measurement of both physical quantities. Problems begin to manifest as one tries to measure materials, in which the effects at the sample-electrode interface start to dominate the total impedance response, making direct measurement of the sample impedance impossible. Overcoming this problem is of vital importance for characterization of solid ion conductors.

The effects at the sample-electrode interface can be avoided by placing voltage measurement electrodes in the bulk of the sample. Since four terminals are used for voltage and current measurements, this technique is called the four-electrode method. Electrical characterization of solid electrolytes has certain peculiarities, which determine the desirable characteristics in an impedance spectrometer:

- The high impedance of current and voltage electrode interfaces to the sample, especially if ion blocking materials are used, necessitates very high common mode and differential input impedances of the differential amplifier.
- Accurate measurements in conditions where the impedance of the sample-electrode interfaces can be several orders of magnitude higher than the impedance of the sample bulk require a very high common mode rejection ratio (CMRR) of the differential amplifier.

- The impedance of the solid electrolyte-electrode interface decreases with increasing frequency, which relaxes the requirements placed on the equipment at high frequencies.
- The impedance of most of the materials being measured has a negligible imaginary part at low frequencies. As a result, scalar measurements may be sufficient for qualitative analysis.
- Because of a complicated equivalent circuit of the system being measured, there is a high possibility of misinterpreting the results. This can be avoided if the bulk impedance of the sample is measured directly.

At the time of this writing, several commercial impedance spectrometers, operating in frequencies ranging from μHz up to a few MHz, are available from Solartron Analytical, Novocontrol, Agilent Technologies, Gamry Instruments, and Autolab. Almost all of these spectrometers operate using the two-electrode method. Of the previously mentioned manufacturers, only Novocontrol offers an impedance measurement system (Alpha-A and Beta Series) that operates using the four-electrode method. However, the capacitance of the differential voltage input is high, reaching 10 pF. Several custom spectrometer designs, capable of four-electrode measurements, exist to investigate liquid[2,3] and solid[4] samples. A four- electrode impedance spectrometer was also introduced by our research group in the past.[5,6]

In this work we present a new impedance spectrometer design, operating in the frequency range of 10 Hz to 2 MHz and capable of performing two- and four-electrode measurements in frequency and time domains, with sample temperatures ranging from 300 K to 800 K. In order to illustrate the capabilities of the spectrometer, measurements of an O^{2-} ion conductor, $Ce_{0.9}Gd_{0.1}O_{1.95}$ (CGO-10), are presented, serving as particularly clear example of the advantages of such setup. It is worth noting, that, despite the fact that the system is originally designed to measure solid electrolyte materials, it is not limited to this application.

---

a)Author to whom correspondence should be addressed. Electronic mail: tomas.salkus@ff.vu.lt.

FIG. 1. Schematic overview of the impedance spectrometer operating in two- and four-electrode measurement modes.

II. EQUIPMENT DESIGN

The impedance spectrometer consists of several distinct components, which are shown in Fig. 1.

The electrical signals are measured by a two channel computer oscilloscope TiePie Handyscope HS3, which has an adjustable resolution (12, 14, or 16 bits) and a built-in function generator. The generated sinusoidal or pulse wave signal is applied to the sample through a buffer. The current through the sample is measured by a current to voltage (*I–V*) converter, which feeds the signal to the first channel (CH1) of the oscilloscope. If four-electrode operation is desired, a differential amplifier is connected to measure the voltage drop on the sample, the output of which is fed through the switch S to the second channel (CH2) of the oscilloscope. Otherwise, two-electrode voltage measurements are taken by connecting the buffer's output to the oscilloscope's CH2 input.

The sample is placed in a custom sample holder. The holder assembly is connected to an Amprobe TMD90A digital thermometer and a custom computer-controlled power supply for the heater, which are used for sample temperature control. All of the control logic of the spectrometer, signal processing, as well as data storage and analysis are implemented in MATLAB software.

Schematic diagram of the two-electrode measurements, utilizing the *I–V* converter, is shown in Fig. 2.

For sample current measurement, an OPA656 high speed JFET input operational amplifier (OA) is connected in a transimpedance amplifier configuration. The gain of this circuit can be controlled by commutation of feedback resistors, which range from 1 kΩ to 16 MΩ.

Theoretical voltage gain of the circuit in Fig. 2 can be written as

$$G_{\mathrm{I}} = \frac{V_{\mathrm{OUT}}}{V_{\mathrm{IN}}} = -\frac{Z_{\mathrm{m}}}{Z_{\mathrm{X}}} \frac{1}{1 + 1/G\beta}, \tag{1}$$

where G is the open loop voltage gain of the OA and $\beta = Z_{\mathrm{x}}/(Z_{\mathrm{m}} + Z_{\mathrm{x}})$ is the feedback factor.

FIG. 2. Schematic diagram of the *I–V* converter.

The actual measurement gain can be written in the form

$$G_m = \frac{V_{\mathrm{CH1m}}}{V_{\mathrm{CH2m}}} = G_{\mathrm{I}}G_{\mathrm{II}}, \tag{2}$$

where G_{II} is the gain of the remaining elements of the measurement circuit, including cables, buffers, attenuators, and the oscilloscope input amplifiers. To take into account these influences, the *I–V* converter is equipped with a calibration circuit, consisting of switches S_1 and S_2, together with a set of resistors R_{k}, which mirror the values of their counterpart, R_m, in the feedback loop. In the case of calibration,

$$G_{\mathrm{k}} = \frac{V_{\mathrm{CH1k}}}{V_{\mathrm{CH2k}}} = -\frac{G_{\mathrm{II}}}{1 + 2/G}, \tag{3}$$

From Eqs. (1)–(3) one can obtain

$$Z_{\mathrm{x}} = \frac{Z_{\mathrm{m}}G_{\mathrm{k}}}{G_{\mathrm{m}}} \left(1 + \frac{G_{\mathrm{k}} - G_{\mathrm{m}}}{(G + 1)\, G_{\mathrm{k}}} \right). \tag{4}$$

The time domain signals V_{CH1m}, V_{CH2m}, V_{CH1k}, and V_{CH2k} are sent to a computer program, where they are converted to the frequency domain utilizing the FFT algorithm. Subsequently, Z_{x} is calculated from Eq. (4).

The equivalent circuit of the sample bulk voltage drop measurement used when operating in the four-electrode mode is presented in Fig. 3.

Here, Z_{x} represents the impedance of the sample segment between the voltage electrodes, V_{g} is the generator output voltage, $V_{\mathrm{x}} = V_{\mathrm{p1}} - V_{\mathrm{p2}}$ is the voltage drop in the sample segment between the voltage electrodes, Z_{e1} and Z_{e2} are the overall impedances of the current electrode-sample interface and sample segments in the regions affected by the current electrodes, Z_{p1} and Z_{p2} are the impedances, introduced by the voltage probe interfaces to the sample, V_{in1} and V_{in2} are the buffer input voltages, C_{dif}, C_{in1}, and C_{in2} are the buffer input differential and common mode capacitances, including the PCB and mounting parasitics, and R_{in1} and R_{in2} are the buffer input resistance. The unity voltage gain of the buffers G_1 and G_2 allows their output signals to be used for active shielding of the assembly and PCB. The buffer's input voltages can be calculated as

$$V_{in1,2} = V_{p1,2} \frac{Z_{in1,2}}{Z_{out1,2} + Z_{p1,2} + Z_{in1,2}}, \tag{5}$$

where $Z_{in1,2}$ is the buffer's input impedances, $Z_{\mathrm{p1,2}}$ are the voltage electrode interface impedances, and $Z_{out1,2}$ are the
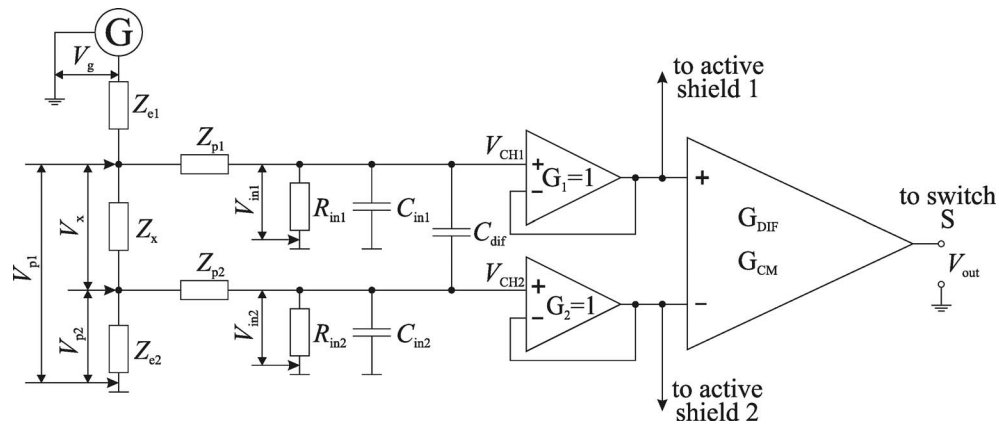
FIG. 3. The sample bulk voltage measurement equivalent circuit.

equivalent output impedances of the virtual voltage sources V_{p1} and V_{p2} (see Fig. 3).

Output voltage can be expressed as

$$V_{out} = \left(V_{p1} \frac{Z_{in1}}{Z_{out1} + Z_{p1} + Z_{in1}} - V_{p2} \frac{Z_{in2}}{Z_{out2} + Z_{p2} + Z_{in2}} \right) G_{DIF}$$

$$+ \left(V_{p1} \frac{Z_{in1}}{Z_{out1} + Z_{p1} + Z_{in1}} + V_{p2} \frac{Z_{in2}}{Z_{out2} + Z_{p2} + Z_{in2}} \right) \frac{G_{CM}}{2},$$

$$(6)$$

where G_{DIF} and G_{CM} are the differential and common mode gains of the differential amplifier, respectively. $Z_{out1,2}$ reaches its maximum value Z_{max} when $Z_x \ll Z_{e1,2}$ and the shunting of

the sample impedance by the buffer inputs is negligible. Then

$$Z_{max} = \frac{Z_{e1} + Z_{e2} + Z_x}{4} = \frac{Z_S}{4}. \quad (7)$$

Here, Z_s is the total impedance of the sample-electrode system. Let $Z_{out1,2} = Z_{max}$, $Z_{p1} = Z_{p2} = Z_p$, and $Z_{in1} = Z_{in2} = Z_{in}$, then

$$V_{out} = \frac{Z_{in}}{Z_S/4 + Z_p + Z_{in}}$$

$$\times \left((V_{p1} - V_{p2}) G_{DIF} + (V_{p1} + V_{p2}) \frac{G_{CM}}{2} \right). \quad (8)$$
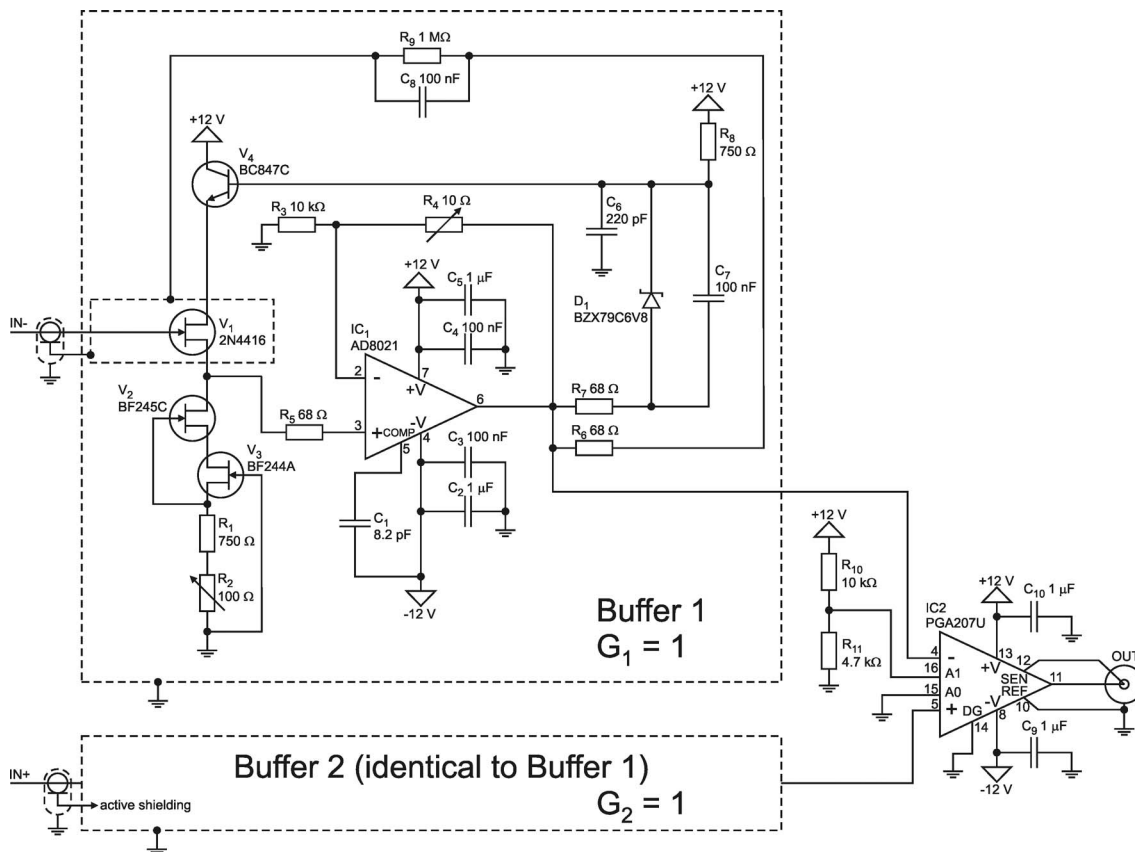
FIG. 4. Schematic of the differential amplifier.
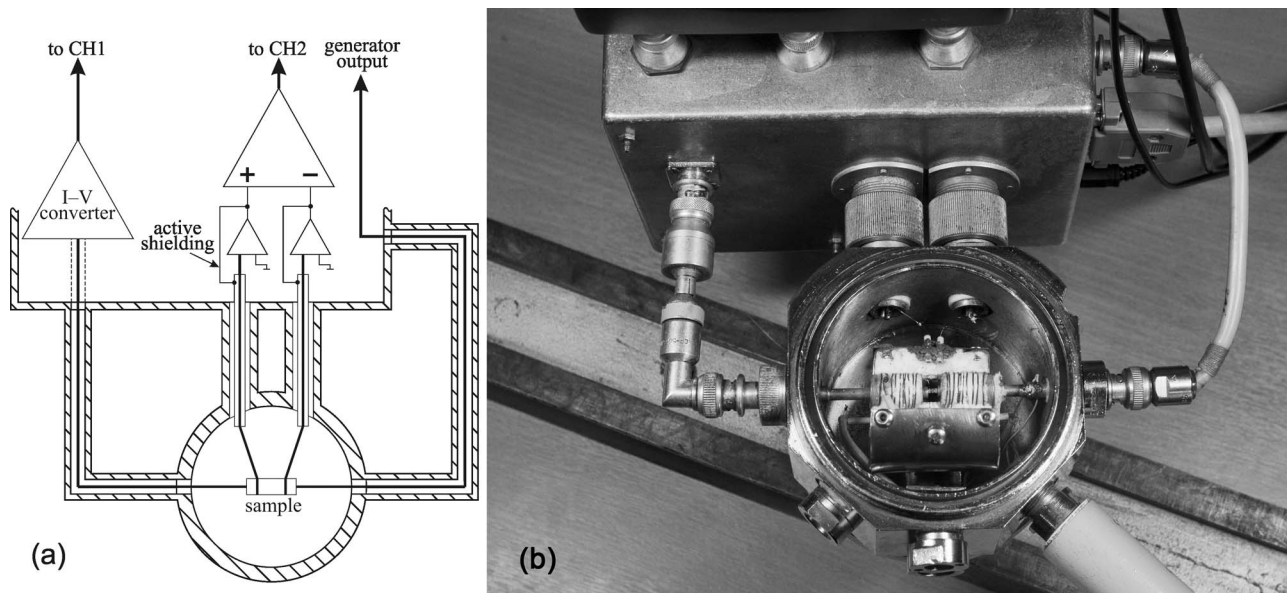
FIG. 5. Schematic view of the sample holder (a) and its photograph (b).

The voltage drop V_x can be calculated from Eq. (8):

$$V_x = \frac{V_{out}}{G_{DIF}}\left(1 + \frac{Z_S/4 + Z_p}{Z_{in}} - \frac{V_{p1} + V_{p2}}{2V_{out}}G_{CM}\right)$$

$$= \frac{V_{out}}{G_{DIF}}(1 + \Delta_V). \tag{9}$$

The current flowing through Z_x is composed of two components – one flowing into the *I–V* converter (I_A) and another flowing into the input of the second buffer:

$$I_x = I_A + \frac{V_{p2}}{Z_p + Z_{in}} = I_A\left(1 + \frac{V_{p2}}{I_A(Z_p + Z_{in})}\right)$$

$$= I_A\left(1 + \frac{Z_{e2}}{Z_p + Z_{in}}\right) = I_A(1 + \Delta_I). \tag{10}$$

From Eqs. (9) and (10)

$$Z_x = \frac{V_{out}}{I_A G_{DIF}}\frac{1 + \Delta_V}{1 + \Delta_I}. \tag{11}$$

Taking the series expansion of $1/(1 + \Delta_I)$ in Eq. (11) and discarding the nonlinear terms, it can be rewritten as

$$Z_x \approx \frac{V_{out}}{I_A G_{DIF}}(1 + \Delta_V - \Delta_I) = \frac{V_{out}}{I_A G_{DIF}}(1 + \Delta), \tag{12}$$

where

$$\Delta = \frac{Z_S}{4Z_{in}} + \frac{Z_p}{Z_{in}} - \frac{Z_{e2}}{Z_p + Z_{in}} - \frac{V_{p1} + V_{p2}}{2V_{out}}G_{CM}. \tag{13}$$

If $\Delta \ll 1$, the unknown impedance is

$$Z_x = \frac{V_{out}}{I_A G_{DIF}}. \tag{14}$$

A differential amplifier with an extremely high input impedance was designed (Fig. 4). The input stage of the buffers G_1 and G_2 was made using a cascode follower consisting of transistors V1 to V4. Two operational amplifiers, IC1 and IC2, present an easy to drive load for the cascode follower circuit, preserving gain accuracy of the buffer.

The characteristics of both circuits were closely matched by choosing a virtually identical pair of 2N4416 JFETs and adjusting the potentiometers R4 and R2. The differential stage consists of a PGA207UA instrumentation amplifier IC3. In order to lower C_{in1}, C_{in2}, and C_{dif}, as well as reduce phase

FIG. 6. Frequency dependences of the differential amplifier's input capacitances.
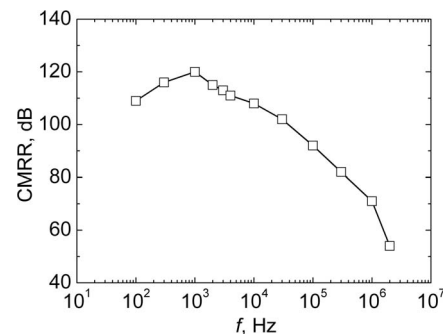
FIG. 7. Frequency dependence of the differential amplifier's CMRR.
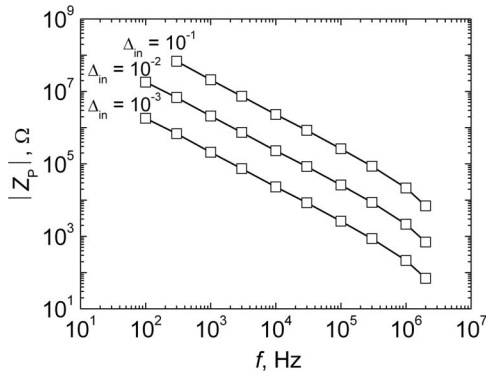
FIG. 8. Frequency dependences of the maximum allowable voltage electrode interface impedance, for different values of Δ_{in}.

errors in current-voltage measurements, the differential amplifier and I–V converter are assembled as close as possible to the sample, as shown in Fig. 5.

Active shields are used to reduce the sample holder parasitic and buffer input capacitances. Frequency dependences of the positive and negative input capacitances of the complete differential amplifier and sample holder setup are shown in Fig. 6. The data were obtained by measuring the attenuation of a RC circuit, formed with the unknown buffer input and sample holder parasitic capacitances C together with known resistances R, connected in series to one of the differential inputs, while the second input was grounded. The input capacitances of both buffers are almost identical. Differential capacitance of the system was found to be $C_{dif} < 0.1$ pF for all frequencies. The input resistances of both buffers were found to be $R_{in1,2} \geq 10^{11} \Omega$. CMRR of the amplifier is shown in Fig. 7.

III. ACCURACY ESTIMATION AND MEASUREMENT

A few assumptions have to be made in order to estimate the spectrometer's accuracy. Let us consider the case in which C_{dif} is negligible. Input impedance is then

$$Z_{in} = \frac{1}{1/R_{in} + i\omega C_{in}}. \tag{15}$$
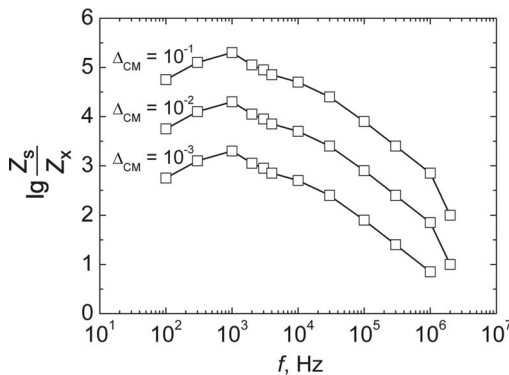
FIG. 9. Frequency dependences of the maximum of $|Z_x|/|Z_s|$, for different values of Δ_{CM}.
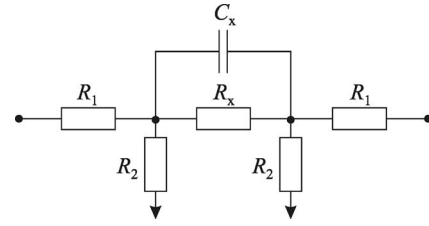
FIG. 10. Circuit used for simulating the solid ion conductor sample, used in the tests of spectrometer accuracy.

Equation (13), which describes the measurement error, can be rewritten as

$$\Delta = \Delta_{in} + \Delta_{CM}, \tag{16}$$

where

$$\Delta_{in} = \frac{Z_S}{4Z_{in}} + \frac{Z_p}{Z_{in}} - \frac{Z_{e2}}{Z_p + Z_{in}} \tag{17a}$$

and

$$\Delta_{CM} = \frac{V_{p1} + V_{p2}}{2V_{out}} G_{CM}. \tag{17b}$$

Δ_{in} describes the error arising from the finite input impedances of the buffers. The relationship $Z_x \ll Z_S$ holds in the vast majority of cases when investigating solid electrolyte materials. In that case, $Z_{e2} \approx Z_S/2$ is also true. If all of the electrodes are made of the same material, $Z_p \approx sZ_S/2$ holds, where $s \gg 1$ is the area ratio of the current and voltage electrodes. This makes the second term of Eq. (17a) the most significant. When these assumptions hold, Eqs. (15) and (17a) can be rearranged into

$$\Delta_{in} \approx Z_p \left(1/R_{in} + i\omega C_{in}\right) \approx \frac{sZ_S}{2} \left(1/R_{in} + i\omega C_{in}\right). \tag{18}$$

This allows us to estimate Δ_{in} using the two-electrode mode of the spectrometer when s is known. Δ_{CM} arises due to the nonidealities of the differential amplifier. In practice, the common mode rejection ratio $CMRR = G_{DIF}/G_{CM}$ is often specified. Noticing that, given $Z_x \ll Z_S$, $V_{p1} + V_{p2} \approx V_g$, Eq. (17b) can be rewritten using this quantity:

$$\Delta_{CM} = \frac{V_g}{2V_{out}} \frac{G_{DIF}}{CMRR} = \frac{V_g}{2V_x} \frac{1}{CMRR} \approx \frac{Z_S}{2Z_x} \frac{1}{CMRR}. \tag{19}$$

The maximum allowable absolute values of Z_p are presented in Fig. 8, as calculated from Eq. (18) for a number of different Δ_{in} values. It is worth noting that the resistance of

TABLE I. Nominal component values used for sample simulation PCBs.

No.	R_x	C_x (pF)	R_1	R_2
1	10 Ω	0	30 kΩ	30 kΩ
2	100 Ω	0	10 kΩ	30 kΩ
3	10 kΩ	0	1 MΩ	3 MΩ
4	100 kΩ	0	1 MΩ	10 MΩ
5	...	4.7	10 kΩ	30 kΩ
6	...	27	10 kΩ	30 kΩ
7	1000 Ω	56	3 kΩ	10 kΩ
8	3 kΩ	27	10 kΩ	30 kΩ

TABLE II. Spectrometer test results, as compared to the commercial impedance measurement equipment.

No.	HP 4284A		This spectrometer, 4-electrode mode		This spectrometer, 2-electrode mode	
	R_x; C_x	Frequency range (Hz)	R_x; C_x	Frequency range (Hz)	R_x; C_x	Frequency range (Hz)
1	10.01 Ω		10.03 Ω	$(10–2) \times 10^5$	10.11 Ω	
2	99.66 Ω		99.20 Ω	$(10–5) \times 10^5$	100.02 Ω	
3	9.994 kΩ	$20–10^6$	9.966 kΩ	$(10–1) \times 10^3$	9.975 kΩ	$(10–2) \times 10^6$
4	99.80 kΩ		99.52 kΩ	$(10–1) \times 10^3$	99.80 kΩ	
5	4.81 pF		5.19 pF	$(80–1) \times 10^4$	4.70 pF	
6	27.7 pF		28.31 pF	$(10–5) \times 10^5$	27.75 pF	
7	999.4 Ω		997.6 Ω	$(10–1) \times 10^6$	1002.7 Ω	
7	56.1 pF		61.2 pF	$2 \times 10^4–2 \times 10^6$	56.5 pF	
8	2.976 kΩ		2.997 kΩ	$(10–2) \times 10^5$	3.001 kΩ	
8	27.7 pF		30.1 pF	$(5 \times 10^3)–5 \times 10^5$	27.75 pF	

the solid electrolyte samples often decreases with increasing frequency. This results in a practical measurement error that increases slower with frequency than $\Delta_{in} \sim f$, as could be observed from Eq. (18) and Fig. 8.

The maximum allowable values of Z_s/Z_x for few fixed values of Δ_{CM} are shown in Fig. 9. The frequency dependency of CMRR is responsible for a rapid decrease in the ratio, as the frequency increases. This can also be seen as an increase in Δ_{CM} with increasing frequency. The reduction of the sample-electrode interface impedance mitigates this effect at high frequencies.

The functionality of the impedance spectrometer was checked by simulating various samples with equivalent circuits of the form shown in Fig. 10.

Each circuit was constructed on a 4×10 mm PCB, using size 0805 surface mount components. The values of the components used for each test case are given in Table I. Before assembling the circuits the resistances of the resistors R_x and the capacitances of the capacitors C_x were measured with a HP 4284A precision LCR meter (from 20 Hz to 1 MHz) as well as the impedance spectrometer, using the two-electrode measurement mode (from 10 Hz to 2 MHz). Frequency dispersion of the measured values was not observed in any of the measurements. The component values, as measured by the commercial equipment and the spectrometer being described, are given in Table II.

The values of R_x and C_x given in Table II are averages over the frequency range indicated. This frequency range corresponds to a measurement using the four-electrode method, in which the absolute deviations from the mean did not exceed 1%. Frequency plots of R_x and C_x values in which the absolute deviations from the mean did not exceed 10% are shown in Figs. 11 and 12, respectively.

It should be noted that the maximum useful frequency for the measurements taken using circuits No. 2, 3, 4, and 8 is limited by the value of the resistor $R2$, which was 30 kΩ, 3 MΩ, 10 MΩ, and 30 kΩ, respectively. This is in excellent correspondence with the values predicted by Fig. 8. The high frequency measurement limit of circuit No. 1 is determined by the ratio of $R_2/R_x = 3000$. The limit of 250 kHz, if the acceptable measurement error is set to be $\Delta_{CM} = 10\%$, is in excellent agreement with the experimental data. In the case of circuit No. 7 and No. 8, the measured capacitance values are slightly increased due to parasitic capacitance between the current electrodes of the sample holder. The current flowing through this capacitance is coupled to the $I–V$ converter directly, bypassing the resistor R_x. Despite the fact that this parasitic capacitance can be easily calculated in normal use due to the simple geometry of the samples (see Ref. 7), it is difficult to determine with any accuracy when testing the spectrometer due to the complicated geometry of the PCB used for this purpose. The low frequency limit for capacitance measurement is determined by the accuracy of the estimation of
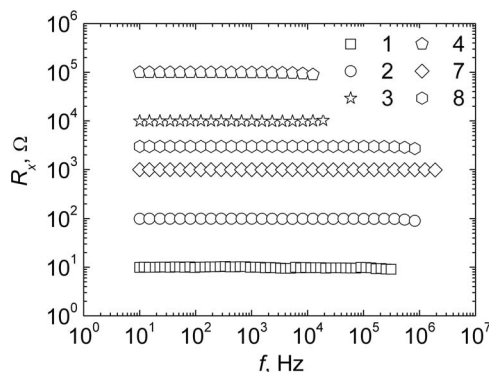

FIG. 11. R_x values in the frequency range where absolute deviations from the mean did not exceed 10%, as measured by the four-electrode method.
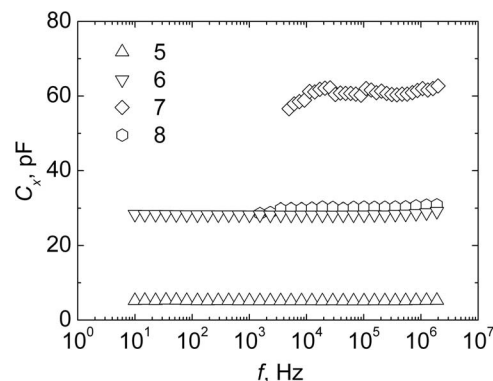

FIG. 12. C_x values in the frequency range where absolute deviations from the mean did not exceed 10%, as measured by the four-electrode method.
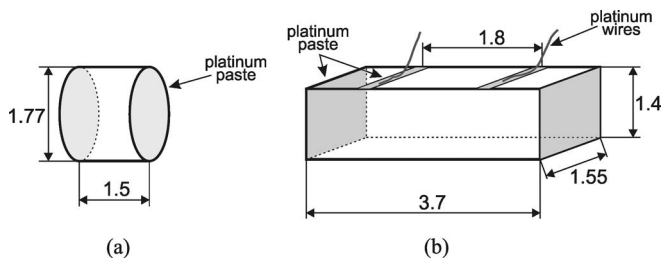
FIG. 13. CGO-10 sample geometry for impedance measurements by the two-electrode (a) and four-electrode (b) methods.

the sample holder capacitance and the measurement phase error, which is $\Delta\phi \approx 0.01°$ for frequencies less than 100 kHz.

IV. TYPICAL SAMPLE PREPARATION AND MEASUREMENT CONDITIONS

A good example to illustrate the advantages of the four-electrode measurements is CGO-10, which is a good oxygen ion conductor.[8] Ceramic samples have been sintered from commercial nano-powder (Fuel Cell Materials) of the material. Electrodes, made of Pt paste (GWENT), were prepared on both end faces of the cylindrical samples used for electrical characterization of the ceramic by the two-electrode method. For measurements by the four-electrode method, parallelepiped shaped samples were prepared. Pt electrodes were deposited for current carrying connections on opposite faces of the sample, together with two strips for voltage measurement on top of the sample. Sample shapes and dimensions (not to scale) are shown in Fig. 13. The voltage measurement points were connected to the spectrometer's differential inputs using Pt wires. While the exact dimensions may vary, the sample shapes presented here are used for most measurements carried out by this spectrometer.

Impedance measurements of the CGO-10 samples were performed by the two-electrode method in the frequency range of 10 Hz to 2 MHz and by the four-electrode method in the frequency range of 10 Hz to 100 kHz. In all cases, the temperature of the CGO-10 ceramic was varied from 300 K

to 710 K in 10 K steps, with each step being stabilized for 2 min with an accuracy of 0.6 K before any measurements of the sample electrical parameters were started. The ac voltage across the sample was 30 mV. All of the measurements were performed in air.

V. TYPICAL RESULTS

Frequency dependences of the real (ρ') and the imaginary (ρ'') parts of complex resistivity at 650 K are presented in Fig. 14(a). Two distinct dispersions of the real part of the resistivity can be observed from the two-electrode measurements. The high frequency (above 100 kHz) dispersion corresponds to oxygen ion migration between the CGO-10 ceramic grains and is usually called the "grain boundary" dispersion. The low frequency dispersion in the $\rho'(f)$ graph is due to the polarization of the interface between the solid electrolyte and the metallic electrode. The maximum in $\rho''(f)$ representation, associated with grain boundary dispersion, is muted, when measured by the two-electrode method despite the fact that it is clearly visible from the four-electrode measurements. The maximum, observed at 1 kHz when using the two-electrode method, is not present in the ρ'' spectrum obtained by the four-electrode method, leading to a conclusion that it is associated with sample-electrode interface. The increase of ρ'' in the low frequency region (<100 Hz) is due to capacitive behaviour of the electrode-electrolyte interface. The low frequency part of ρ', obtained by the four-electrode method, does not exhibit any frequency dependence and ρ'' shows no increase at the lowest frequencies.

A conventional way to present and analyze impedance spectra is the complex plane plot of $\rho''(\rho')$. In the resistivity complex plane plot of CGO-10, measured at 650 K (Fig. 14(b)), the spectrum obtained by the two-electrode method indicates a sizeable influence of several processes at the interface between the electrode and the electrolyte (the response of double layer capacitance, diffusion, or possible chemical reactions). In this case the extraction of the grain boundary resistance values (ρ_{gb}) from the measurement by the two-electrode method is not possible without complex
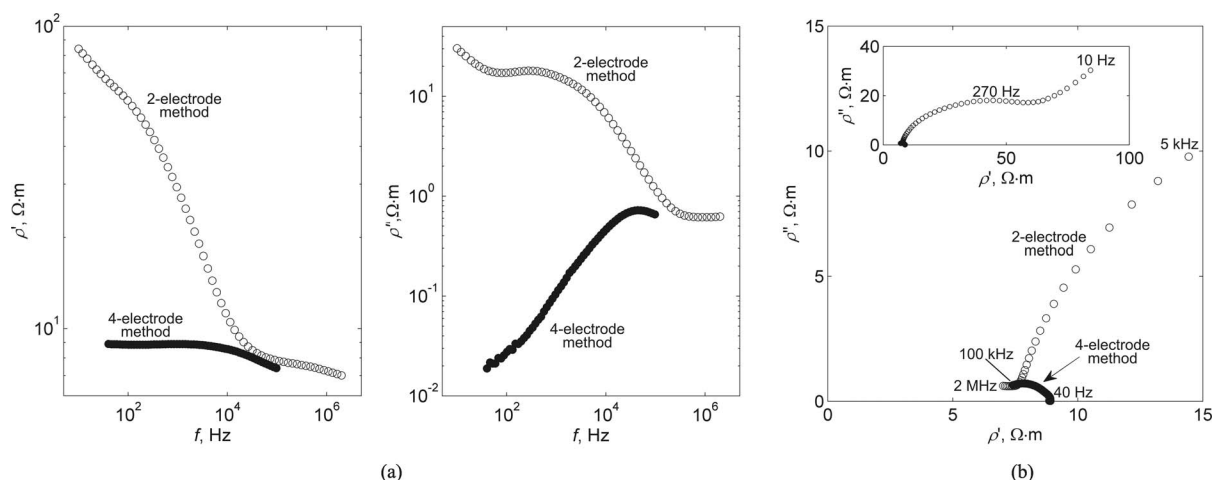

FIG. 14. Frequency dependences of the real and the imaginary parts of complex resistivity (a) and complex plane plot of resistivity (b), measured at 650 K of CGO-10 ceramics. Inset in (b) shows full frequency range.

theoretical modelling of the ceramic sample, while the grain boundary conductivity can be easily ascertained from the four-electrode measurement, due to the spectrum not being influenced by the electrode. The diameter of the semicircle corresponds to ρ_{gb}. The simplicity of the impedance spectra, obtained by the four-electrode method, considerably reduces the chance of misinterpretation of the data.

VI. CONCLUSIONS

A computer controlled impedance spectrometer, capable of performing two- and four-electrode measurements, has been designed and built. Operating frequencies of the device range from 10 Hz to 2 MHz, while the temperature of the sample can be adjusted and stabilized in the range of 300 K to 800 K. The spectrometer is able to measure samples having an impedance in the range of 10 Ω to 10 GΩ. The four-electrode measurement capabilities of the spectrometer allow direct and accurate measurement of ionic conductor electrical properties when ion blocking electrodes are used.

[1] J. R. Macdonald, *Impedance Spectroscopy* (Wiley-Interscience, New York, 1987), p. 595.
[2] D. Pelc, S. Marion, and M. Basletić, Rev. Sci. Instrum. **82**, 073907 (2011).
[3] B. A. Mazzeo and A. J. Flewitt, J. Appl. Phys. **102**, 104106 (2007).
[4] P. Kurek and G. Fafilek, Solid State Ionics **119**, 151 (1999).
[5] A. Orliukas, A. Kežionis, V. Mikučionis, and R. Vaitkus, Elektrochimija **23**(1), 98 (1987).
[6] A. Kezionis, A. Orliukas, K. Paulavicius, and V. Samulionis, Mater. Sci. Forum **76**, 229 (1991).
[7] A. F. Orliukas, A. Kezionis, and E. Kazakevicius, Solid State Ionics **176**, 2037 (2005).
[8] K. Huang, M. Feng, and J. B. Goodenough, J. Am. Ceram. Soc. **81**(2), 357 (1998).